FEATURE EXTRACTION AND CLASSIFICATION IN AUTOMATED INSPECTION OF NDE IMAGES

Zhong Zhang and John P. Basart
Center for Nondestructive Evaluation and
Dept. of Electrical Engineering and Computer Engineering
Iowa State University
Ames, IA 50011

INTRODUCTION

Industry currently relies on manual inspection of X-Ray images, which is expensive, time consuming and subject to inconsistent results by various inspectors. Automatic inspection of the industrial NDE images using high speed computers would make the flaw detection task more consistent and efficient. However, since the objects to be inspected usually have complex geometric structures, it is very difficult to separate automatically flaws from the complex geometric background of an image. Most of the automated inspection systems developed so far are customized packages which are tailored for particular types of applications, such as the inspections of aluminum wheel castings [1], the welds of space shuttle fuel tanks [2], and nodules in chest X-rays [3]. Customized packages have the advantages of relatively fast speed and good liability, but they can not be used in other applications without substantial changes in computer programs.

In this paper, we introduce a general purpose automated flaw detection approach in the inspection of industrial radiographs. It is a general purpose image segmentation approach that can be used in other imaging modalities. It first extracts the local features of an image from a multiple-level decomposed wavelet transform of the image, then classifies the image features by a supervised adaptive fuzzy logic classifier. Since the supervised fuzzy classifier is built on the training prototypes of a specific application, customization for that application is therefore established through the training process. Figure 1 shows a simplified block diagram of the automated inspection system.

WAVELET FEATURE EXTRACTION

Feature extraction through spatial/spatial-frequency analysis of an image has been very popular in machine vision applications because studies in neural biology indicate that the human/biological visual system is performing local spatial frequency analysis through sets of band-pass filters [4-5]. The most commonly used spatial filters in image segmentation are windowed Fourier filters and Gabor filters [6]. But both filters are bounded by the Heisenberg uncertainty principle [7-9]. Therefore, they can not be localized in both the spatial and spatial-frequency

Review of Progress in Quantitative Nondestructive Evaluation, Vol. 14
Edited by D.O. Thompson and D.E. Chimenti, Plenum Press, New York, 1995

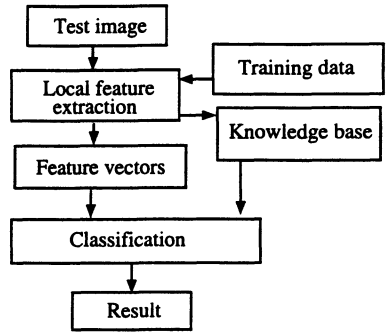

Fig. 1 Simplified block diagram of an automated flaw detection system.

domains, which makes feature extraction based on the windowed Fourier and Gabor filter banks complicated and computationally expensive. The wavelet transform is an alternative spatial/spatial-frequency analysis. It can also be localized in both the spatial and transformed domains because it sacrifices continuity in exchange for localization [10]. It is also a multiresolution analysis which provides contextual information of images. Therefore, it is very attractive to use the wavelet transform in extraction of image local features.

To extract local features, we conduct a normalized Daubechies 4 wavelet transform [11], which is the most compactly supported wavelet transform, to a certain level of decomposition in the pyramid structure. The normalization is in the sense that the transform is the same amplitude for high and low frequency signals of the same amplitude. As sketched in Fig. 2(b), for a two dimensional image, a first level wavelet decomposition results in four smaller versions of the original image in Fig. 2(a), marked as "ss", "sd", "ds", "dd" in the figure to indicate smoothing and decomposition in horizontal and vertical directions, respectively. Since the transform is localized, for every pixel of interest in the original image, we can point out one "smoothed" value in "ss" region and three "decomposed" values in regions associated with "d" in the transformed domain. We use the smoothed value as one feature to indicate the basic tone of the image, then compare the decomposed values and use the maximum magnitude as another feature to represent the dominant frequency (or scale) at that level. Similarly, for a second level decomposition shown in Figure 2(c), in which the capital letters indicate second level smoothing and decomposition. Note the pattern of second level decompositions. The upper left quadrant of Fig. 2(b) has been decomposed in both directions, the lower right quadrant of Fig. 2(b) not decomposed at all, and upper right and the lower left quadrants of Fig. 2(b) are decomposed in one direction only. There are totally nine values in the transformed domain of Fig. 2(c) related to the pixel of interest in the original image. The dominant frequency at this level is found by choosing the maximum magnitude among related values in all decomposed regions associated with "D" and "d", and is used as the third feature in the feature vector. The decomposition and feature extraction are continued to a higher level until a desired size of feature vector is reached.

An example of this feature extraction is shown in Fig. 3. The original image is an X-ray radiograph of a weld with a gas hole flaw. The feature extraction starts at the second level de-

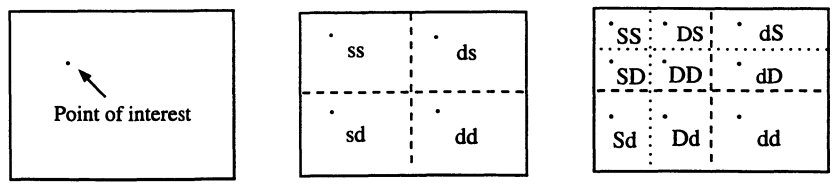

(a) Original image (b) Level 1 decomposition (c) Level 2 decomposition

Fig. 2 Sketch of wavelet decompositions of an image.

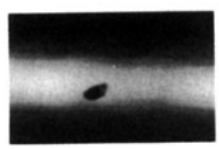

(a) Original image

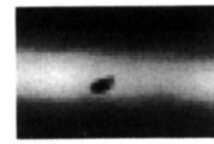

(b) 2nd level smoothed feature

(c) 2nd level decomposed feature

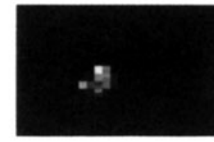

(d) 3rd level decomposed feature

Fig. 3 Weld image and its feature maps.

composition of the original image. Fig. 3(b) displays the 2nd level smoothed feature, 3(c) displays the feature extracted from second level decomposition and 3(d) shows the feature extracted from third level decomposition. It is clearly shown in Fig. 3 that features extracted from wavelet decomposition give multiresolution representations of the original image.

SUPERVISED ADAPTIVE FUZZY CLASSIFICATION

After feature extraction, feature vectors associated with image pixels are classified by a supervised fuzzy logic classifier established through the training prototypes. Unlike a conventional backpropagating neural network, which is a "black box" initiated from random numbers and converges slowly, a fuzzy system starts from fuzzy rules directly derived from the training prototypes, or linguistic rules from human experts. It uses fewer steps in training and is also proven to be a universal approximator [12]. There are four functional parts in the supervised fuzzy classifier, namely, fuzzification, knowledge base, fuzzy inference and defuzzification. The inputs to the classifier are nonfuzzy feature vectors. The fuzzification provides the interface from the crisp input to the fuzzy system by establishing input fuzzy sets and their membership functions. The fuzzy inference is the decision making logic that generates the output fuzzy sets, and the defuzzification is another interface which summarizes the output fuzzy sets and provides crisp system output. The knowledge base of the system contains the prototype training data and/or the linguistic rules for the classification. It is clear that a fuzzy system provides a nonlinear mapping from a crisp input to a crisp output, while fuzzy reasoning and the knowledge base control the performance of the system.

ADAPTIVE TRAINING

The knowledge base controlling the behavior of the classifier is initiated from the training data. Suppose there are M vectors of size N in the training data file, each of the vectors is assigned a desired output label value, in the following form:

Training prototype feature values x_{ij} Desired output

$$
\begin{aligned}
&x_{11}, x_{21}, x_{31}, \cdots x_{N1} \longrightarrow d_1 \\
&x_{12}, x_{22}, x_{32}, \cdots x_{N2} \longrightarrow d_2 \\
&\quad \cdots \qquad\qquad\qquad\quad \cdots \\
&x_{1M}, x_{2M}, x_{3M}, \cdots x_{NM} \longrightarrow d_M
\end{aligned}
$$

where the subscripts *ij* are feature and vector indices, respectively. If there are not duplicated items, each vector and its desired output value in the training data file lead to a fuzzy rule in the fuzzy rule base. The membership function for the *i*th feature in the *j*th rule, denoted as μ_{ij}, is given by a unit-amplitude Gaussian form as

$$\mu_{ij}(x_i) = \exp\left[-\frac{(x_i - x_{ij})^2}{2\sigma_{ij}^2}\right] \tag{1}$$

in which the center of the membership function is initialized at the training prototype position x_{ij} and the standard deviation σ_{ij}, which is used to control the effective range of the membership function, is derived from the range of each feature in the training data file as

$$\sigma_{ij} = \frac{\max(x_{ij}) - \min(x_{ij})}{const}, \; j = 1, 2, \cdots M, \textit{ for every } i. \tag{2}$$

In our application, if we have an input feature vector $\mathbf{X} = (x_1, x_2, \ldots x_N)'$, its output fuzzy membership (the degree of belonging) to each fuzzy rule is given by multiplying its input membership functions associated with that rule. That is, the degree that vector $\mathbf{X}$ belongs to rule j is given as:

$$D_j(\mathbf{X}) = \mu_{1j}(x_1) \cdot \mu_{2j}(x_2) \cdots \mu_{Nj}(x_N) = \prod_{i=1}^{N} \mu_{ij}(x_i). \tag{3}$$

The system output for any input vector $\mathbf{X}$ is given by the centroid defuzzification method which is a normalized sum of all the elements of the output fuzzy set:

$$f(\mathbf{X}) = \frac{\sum_{j=1}^{M} d_j D_j(\mathbf{X})}{\sum_{j=1}^{M} D_j(\mathbf{X})} = \frac{\sum_{j=1}^{M} d_j \left[\prod_{i=1}^{N} \mu_{ij}(x_i)\right]}{\sum_{j=1}^{M} \left[\prod_{i=1}^{N} \mu_{ij}(x_i)\right]} \tag{4}$$

where N is the size of feature vector, M is the total number of rules applied and the centroid of the output fuzzy set d_j is initialized from the desired output value for the jth rule.

Once fuzzy rule base and membership functions have been established, system output can be computed from Equation (4) for any input feature vector in the training data file. The output error e is defined by the difference between f($\mathbf{X}$) and the desired output. A least square error training is then achieved for the system by a steepest descent iteration which reshapes the input and output fuzzy membership functions by updating the means and the standard deviations of Equation (1) and the centroid of the output fuzzy set d_j until the error is minimized. This is given by

$$\begin{aligned} x_{ij}(k+1) &= x_{ij}(k) - \alpha \frac{\partial e^2}{\partial x_{ij}}, \\ \sigma_{ij}(k+1) &= \sigma_{ij}(k) - \alpha \frac{\partial e^2}{\partial \sigma_{ij}}, \\ d_j(k+1) &= d_j(k) - \alpha \frac{\partial e^2}{\partial d_j}, \end{aligned} \tag{5}$$

where α is the step size and k is the number of iteration.

EXPERIMENTAL RESULTS

Automated image segmentation is done pixel-wise. One set of test images consists of gas hole flaws in welds. Three features shown in Figures 3(b), 3(c) and 3(d) are used in the feature vector. The training is conducted through user's interactive input on a computer screen. The flaw detection package runs on UNIX platforms and has an X-Window graphic user interface. A user uses a mouse to draw in the sample images to indicate flaw prototype pixels and background prototype pixels. The feature vectors of pixels chosen by the user are computed and stored in a training data file. The system needs to be trained from the training data before it can be used. When a training process begins, the program reads the training data from the file and discards duplicated items, then it updates the membership functional parameters iteratively until

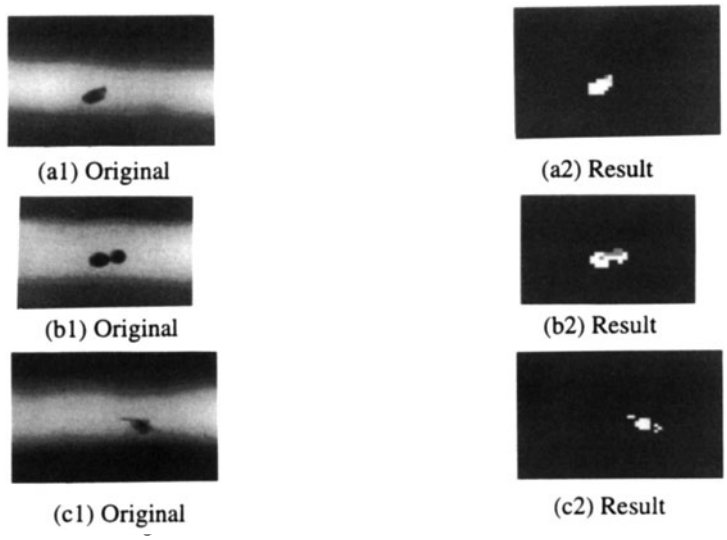

Fig. 4 Detection of gas holes in welds.

the error is minimized. This is actually the establishment of the knowledge base (fuzzy rule base) that controls the performance of the classifier and usually takes less than 1 second on a DEC 5000/200 workstation to finish the training. Once the training process is completed, the fuzzy rule base is loaded into the memory and the classifier is ready. Figure 4 shows the testing results of images with gas hole flaws in welds. Original images are displayed on the left column and the classification results are displayed on the right. Several pixels in the flaw area in Figure 3(a) were used as flaw prototypes and pixels on a single slice across the image background were used as background prototypes. The results show that flaws (white area) are distinguished from the background (black area), and the grays in the output image indicate the classification of unknown prototypes that are not included in the training knowledge base. Figure 5 displays the inspection results of images with heavy inclusions in welds that are different from gas hole flaws. Again, left side images are original and right side images are the results, the training prototypes of flaws are obtained from several isolated pixels in the bright "noise like" flaw spots in Figure 5(a1), and background prototypes are assigned from pixels on a single slice in the image background. The system detects the inclusion flaws and marks them in white. The flaws do not exist in the training data file are also found but are marked in gray. While the background pixels of the images are marked in black in the output images.

CONCLUSION

An image segmentation approach based on local feature extraction and supervised classification has been developed to detect flaws automatically in NDE images. Features are extracted from a compactly supported 2 dimensional wavelet transform of the image because the wavelet transform is the only spatial/spatial frequency analysis that can be localized in both the spatial and transformed domains. Commonly used Gabor filters and other windowed Fourier analysis methods can not be localized in both domains. Consequently, a windowed operation must be performed on the data which is time consuming and often loses information. In addition, because the pyramid structure of the wavelet decomposition allows fast computation of the transform, the feature extraction processes is several times faster than conventional windowed approaches. Wavelet transform inherently defines various sized windows in the transform and the computation does not need to be done window by window. All local features are extracted through one process. Pixel-wise image segmentation is achieved by classifying local features with a supervised adaptive fuzzy classifier. Compared to a conventional backpropagating neural network, which is a "black box" and very slow in the training stage, the training process of the fuzzy classifier is much faster because it is established directly from the training data file. An

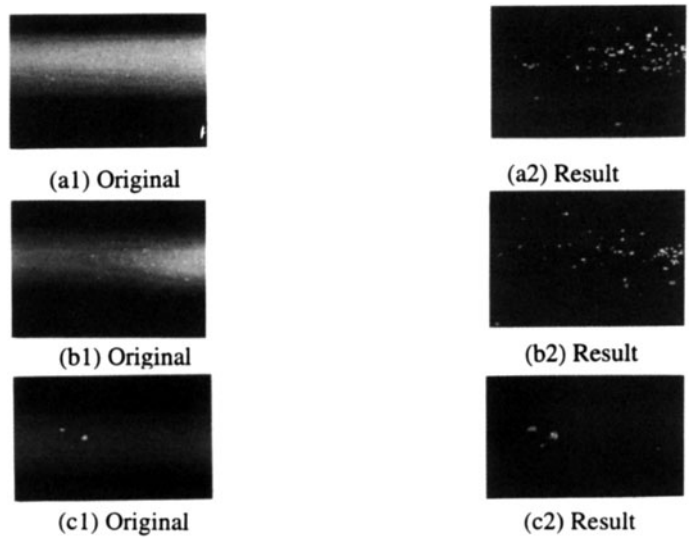

Fig. 5 Detection of inclusions in welds.

X-window graphic user interface has been built for this software package allowing a user to easily perform complicated training processes and classification tasks. The performance of the system depends on the completeness of the knowledge base. Our future work lies in the optimization of the fuzzy rule base of the classifier and the establishment of a confidence measure in flaw detection.

ACKNOWLEDGMENT

The authors thank the Center for NDE of Iowa State University for supporting this work.

REFERENCES

1. H. Boerner, and H. Strecker, "Automated X-ray inspection of Aluminum castings," IEEE Trans. Pattern Anal. Machine Intell., vol. 10, pp. 79-91, 1988.
2. J. P. Basart, and J. Xu, "Automatic detection of flaws in welds," Technical Report, Center for NDE and Dept. EECpE, Iowa State University, 1991.
3. C. Gatot, "Feature extraction in medical radiographic images," M.S. thesis, Iowa State University, 1988.
4. J. J. Kulikowski, S. Marcelja, and P. Bishop, "Theory of spatial position and spatial frequency relations in the receptive fields of simple cells in the visual cortex," Biol. Cybern., vol. 43, pp. 187-198, 1982.
5. D. A. Pollen, and S. F. Ronner, "Spatial computation performed by simple and complex cells in the visual cortex of the cat," Vision Research, vol.. 22, pp. 101-118, 1982.
6. D. Gabor, "Theory of Communication,", J. IEE, vol. 93, pp. 429-457, 1946.
7. A. Bovik, M. Clark, and W. Geisler, "Multichannel texture analysis using localized spatial filters," IEEE Trans. Pattern Anal. Machine Intell., vol. 12, pp. 55-73, 1990.
8. A. K. Jain, and F. Farrokhnia, "Unsupervised texture segmentation using Gabor filters," Pattern Recognition, vol. 23, pp. 1167-1186, 1991.
9. J. Bigun, and J. M. H. du Buf, "N-folded symmetries by complex moments in Gabor space and their application to unsupervised texture segmentation," IEEE Trans. Pattern Anal. Machine Intell., vol. 16, pp. 80-87, 1994.
10. O. Rioul and M. Vetterli, "Wavelets and signal processing," IEEE Signal Processing Magazine, pp. 14-38, Oct. 1991.
11. I. Daubechies, *Ten Lectures on Wavelets*, SIAM, Philadelphia, 1992.
12. L. Wang, and J. M. Mendel, "Fuzzy basis functions, universal approximation, and orthogonal least-square learning," IEEE Trans. Neural Networks, vol. 3, pp. 807-814, 1992.